

Metamagnetism and tricriticality in heavy-fermion ferromagnet URhGe

A. S. Gubina¹ and M. E. Zhitomirsky^{1,2}

¹*Université Grenoble Alpes, CEA, IRIG, PHELIQS, 38000 Grenoble, France*

²*Institut Laue Langevin, 38042 Grenoble Cedex 9, France*

(Dated: October 22, 2024)

URhGe is a ferromagnetic superconductor with a distinctive magnetic behavior. In a field $H \parallel b$ applied perpendicular to the easy axis, URhGe exhibits an abrupt orientational transition of the magnetization with a reentrant superconducting phase emerging close to the transition field H_m . We develop a theoretical description of the magnetic properties of URhGe by considering a spin model with competing magnetic anisotropies. The model is analyzed both analytically at zero temperature and with Monte Carlo simulations at finite temperatures. The constructed H_b - T phase diagram features a tricritical point on the line $H_m(T)$ and is in a good quantitative agreement with the experimental diagram of URhGe. We demonstrate that the asymptotic tricritical behavior of the order parameter and the correlation length is described by the mean-field critical exponents. The derived microscopic parameters suggest that URhGe is an XY-like ferromagnet with an additional weak in-plane anisotropy in the bc plane.

I. INTRODUCTION

It is generally accepted that ferromagnetism is detrimental to superconductivity. The discovery of coexisting superconducting and ferromagnetic phases in the heavy fermion materials UGe₂ [1], URhGe [2], and UCoGe [3] challenges this common perception. The exact mechanism responsible for the simultaneous presence of two antagonistic states is still a matter of debate, see [4–10] for theoretical discussions and [11–13] for general overviews. To make progress, a deeper understanding of the magnetic properties of these uranium compounds is required. In our work, we focus on URhGe, in which superconductivity and ferromagnetism are present at ambient pressure. Interestingly, URhGe has a second superconducting pocket in a strong magnetic field $H \parallel b$ [14]. The reentrant superconducting phase resides in the vicinity of the metamagnetic transition at $H_m = 11.7$ T, which corresponds to a discontinuous rotation of the ferromagnetic moment from a tilted orientation to the field direction.

Theoretical description of U-based intermetallic magnets is complicated by the dual nature of $5f$ electrons that demonstrate both itinerant and localized character, see, *e.g.*, [15, 16]. Magnetic moments are thought to be well localized in UGe₂, which has a high Curie temperature $T_C \sim 52$ K and large ordered moments $m_0 \sim 1.5\mu_B$ per U atom. UCoGe with $T_C \sim 2.4$ K and $m_0 \sim 0.06\mu_B$ is considered as the most itinerant among three materials. An intermediate situation is found for URhGe, which has $T_C = 9.5$ – 9.7 K [2, 17] and $m_0 = 0.41\mu_B$ [14]. The Shubnikov-de Haas [18], the Hall conductivity [19], and the thermoelectric power [20] measurements indicate that a Fermi surface reconstruction takes place in URhGe close to H_m . Based on this observation, an interpretation of H_m as a field-induced Lifshitz transition was made in several studies [18–21], though no consistent explanation of the magnetic properties was obtained within the itinerant scenario. Note that the reduced value of U moments in URhGe is, at least, partly related to antiparallel locking of orbital and spin moments of $5f$ electrons

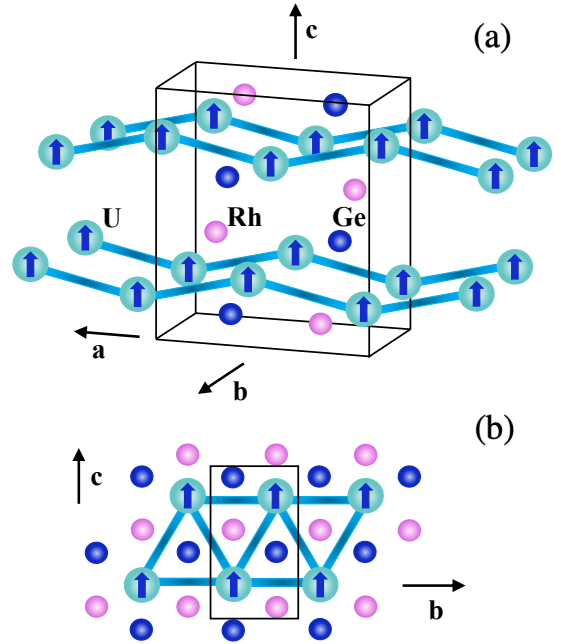


FIG. 1. Crystal lattice of URhGe. (a) General view, the rectangular prism shows the unit cell. (b) Projection along the a axis. Only the U atoms with coordinates $x \approx 0$ are included, the shown Rh and Ge atoms are positioned near to the $x = 0.2$ plane.

due to the strong spin-orbit coupling [22, 23].

In this work, we adopt a local-moment description of the magnetic subsystem in URhGe. Our approach is based on the following experimental facts that are hardly consistent with the itinerant picture. First, the magnetic susceptibility along three principal directions follows the Curie law in a wide range of temperatures below 300 K [24]. Second, the net in-plane magnetization $\sqrt{m_b^2 + m_c^2}$ stays almost constant through the metamagnetic transition H_m [14]. Furthermore, the X-ray magnetic circular

dichroism measurements indicate that $\sim 80\text{--}90\%$ of the total magnetization of URhGe is determined by the 5*f* electrons localized on the U atoms [23]. A weak, nearly isotropic growth of the magnetization observed in strong magnetic fields $H \parallel bc$ [14] can be attributed to the residual contribution of the conduction bands.

URhGe has the orthorhombic TiNiSi-type crystal structure corresponding to the *Pnma* space group [15, 24]. The lattice is formed by zigzag chains of U atoms that propagate along the *a* crystallographic direction, Fig. 1. The TiNiSi lattice is a derivative of the high-symmetry hexagonal AlB₂-type structure [25]. The connection becomes transparent for the projection along the *a* direction, which is parallel to the six-fold axis of the hexagonal lattice, see Fig. 1(b). Accordingly, there is a large disparity in magnetic properties of URhGe between the *a* axis and two orthogonal directions. Indeed, at temperatures close to T_C , the magnetic susceptibility χ_a is an order of magnitude smaller than $\chi_{b,c}$. The difference between χ_b and χ_c is further determined by a weak in-plane anisotropy.

The abrupt orientational transition in URhGe is a rare case among easy-axis ferromagnets. Usually, magnetic moments rotate continuously in an applied field until a full alignment is reached at the second-order transition field. Such a behavior is highlighted by the transverse-field Ising model, which often serves as a paradigmatic example of the Z_2 quantum critical point [26]. Nonetheless, the first-order transition in a transverse magnetic field can be induced by higher-order harmonics in the angular dependence of the magnetocrystalline anisotropy [27]. Such a mechanism has been used to explain the first-order magnetization processes in various ferromagnetic alloys, see, *e.g.*, [28].

For an orthorhombic ferromagnet the energy density as a function of angle θ measured from the easy axis towards an intermediate one is expanded as

$$\mathcal{E} = K_1 \sin^2 \theta + K_2 \sin^4 \theta + \dots \quad (1)$$

with $K_1 > 0$. If only the two leading terms are kept in (1), the first-order transition in magnetic field can appear for negative K_2 , see [27] and Sec. III.

The LSDA calculations of the magnetic anisotropy for URhGe show a good agreement with Eq. (1) predicting a fairly large value of the second harmonic: $K_2/K_1 \approx -0.66$ [29]. A possible link between the complex form of magnetic anisotropy and the first-order reorientation process has been suggested in [30], though no explicit calculations were provided. A phenomenological description of URhGe based on the Landau expansion for an orthorhombic ferromagnet was formulated in several works [14, 31, 32]. However, such a description is not entirely consistent. The metamagnetic transition in URhGe takes place at low temperatures and in high magnetic fields, which are beyond the scope of the Landau theory.

Below, we follow an alternative approach and formulate a simple microscopic model, which is suitable to study both magnetic statics and dynamics of URhGe.

In this article, we focus on the static properties and, in particular, explain a high sensitivity of the metamagnetic transition to the applied field orientation [33, 34] as well as obtain location of the tricritical point on the transition line $H_m(T)$ [20, 35]. The paper is organized as follows. Section II outlines a spin model chosen for URhGe. A zero-temperature analysis of the model is presented in Sec. III. Section IV describes the finite-temperature properties, the tricritical point, and the H - T diagram obtained with the help of the classical Monte Carlo simulations. The obtained results are summarized in Sec. V. The supplemental zero-field Monte Carlo data are included in Appendix.

II. MICROSCOPIC SPIN MODEL

Quantum effects play a little role in three-dimensional ferromagnets. Therefore, we use a classical spin model with unit length spins \mathbf{S}_i representing uranium moments. Our consideration is based on the following spin Hamiltonian

$$\hat{\mathcal{H}} = - \sum_{\langle ij \rangle} J_{ij} \mathbf{S}_i \cdot \mathbf{S}_j + \hat{\mathcal{H}}_a - \mathbf{H} \cdot \sum_i \mathbf{S}_i. \quad (2)$$

The first term corresponds to the exchange interactions between uranium moments. Magnetic anisotropy is accounted for by the single ion term $\hat{\mathcal{H}}_a$, although anisotropic exchange interactions may also be present in uranium intermetallics. Finally, the Zeeman energy is taken in a simplified form by absorbing an anisotropic g factor and μ_B into a magnetic field value H .

The single-ion energy is taken as

$$\hat{\mathcal{H}}_a = \sum_i \left[D S_i^{x2} + E (S_i^{y2} - S_i^{z2}) + K (S_i^y)^2 (S_i^z)^2 \right], \quad (3)$$

where x, y, z are chosen along a, b, c , respectively. The first two terms in (3) is a standard bi-axial anisotropy compatible with the point symmetry group on magnetic sites [36]. The hard and the easy magnetization directions along the *a* and the *c* crystallographic axes correspond to $D \gg E > 0$, in accordance with the susceptibility measurements [37] and the LSDA calculations [29]. The last term in Eq. (3) generates the four-fold θ -harmonic in the macroscopic energy density (1). The choice of a microscopic interaction responsible for the $\sin^4 \theta$ harmonic is to some extent arbitrary. Any appropriate quartic combination of the two spin components can be equivalently chosen for $\hat{\mathcal{H}}_a$. Also, anisotropic biquadratic interactions can be at the origin of such anisotropy and their effect on the thermodynamics will be indistinguishable from the K -term as long as the system has extended ferromagnetic correlations.

The local symmetry on U sites in the crystal lattice of URhGe consists of the mirror reflection σ_y only. Hence, $\hat{\mathcal{H}}_a$ may also include a term $\pm(S_i^x S_i^z + S_i^z S_i^x)$ alternating in sign between four U atoms in the unit cell Fig. 1. As

a result, a uniform ferromagnetic alignment of spins parallel to the z direction can be accompanied by staggered spin components along x . The neutron diffraction experiments do not detect such spin staggering in the ordered state [2, 38]. Hence, we omit the corresponding term in Eq. (3).

Absence of the staggered term in $\hat{\mathcal{H}}_a$ makes four U atoms in a unit cell equivalent and allows us to map the real crystal structure onto an orthorhombic Bravais lattice. We assume exchange interactions between the nearest neighbors only. Furthermore, exchange constants along three crystal directions are replaced by an averaged exchange parameter $J = (1/z) \sum_j J_{ij}$. The Monte Carlo results included in Appendix show that the transition temperature of an orthorhombic Heisenberg ferromagnet depends only weakly on an ‘orthorhombic distortion’ of the exchange constants. Thus, a simplified modelling of an (unknown) three-dimensional exchange pattern in URhGe with a single parameter J does not introduce a significant quantitative error.

III. ZERO TEMPERATURE

In this section we consider the magnetization process in an external field applied parallel to the crystallographic bc -plane. At zero temperature, spins are confined to the yz -plane and remain to be parallel to each other. Dropping an unimportant constant from the total energy \mathcal{E} , we write it as a function of an angle θ between the net magnetization \mathbf{M} and the z axis:

$$\mathcal{E}/N = (2E + K) \sin^2 \theta - K \sin^4 \theta - H \sin(\theta + \alpha). \quad (4)$$

Here α is an angle between an external field and the y axis. Comparison of Eqs. (1) with (4) relates the macroscopic and microscopic anisotropy parameters by $K_1 \rightarrow (2E + K)$ and $K_2 \rightarrow -K$.

For small K , the energy in zero field increases monotonously from the minimum value at $\theta = 0$ to the maximum at $\theta = \pi/2$. For $K > 2E$ ($K_2/K_1 < -0.5$), the orthogonal orientation $\theta = \pi/2$ changes to a local minimum, whereas a maximum shifts to $\sin^2 \theta_0 = (2E + K)/2K$. In such a situation there is clearly a first-order transition in the transverse magnetic field, where the equilibrium angle θ jumps from an intermediate value to $\theta = \pi/2$. In the following subsection we derive an exact condition for the development of a first-order jump, which extends considerably the range of relevant K values in comparison to $K > 2E$.

A. H along the b axis

The minimum energy condition applied to Eq. (4) yields for $\alpha = 0$:

$$2(K + 2E) \sin \theta - 4K \sin^3 \theta - H = 0. \quad (5)$$

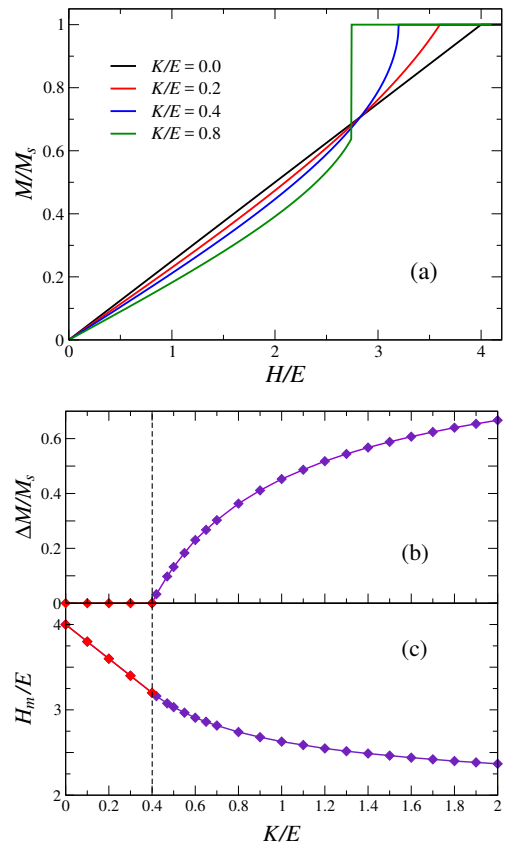


FIG. 2. (a) Magnetization curves for $H \parallel y$. Here, $M = M_y$ and $M_s = |\mathbf{S}|N$ is the total magnetisation. (b) The relative magnetization jump and (c) the critical field as a function of K/E .

For $K = 0$, the magnetization tilts continuously from the easy direction with $\sin \theta = H/H_m$ until a full alignment is reached at the second-order transition field $H_m = 4E$. For finite $K > 0$, rotation of spins remains continuous as long as the cubic equation obtained from Eq. (5):

$$f(x) = ax - bx^3 - H = 0, \quad x = \sin \theta, \quad (6)$$

has only a single root for all $H > 0$ in the physical domain $0 \leq x \leq 1$. By expanding the energy (4) near $x = 1$ we obtain that the second-order transition shifts as $H_m = 4E - 2K$ by the extra in-plane term in $\hat{\mathcal{H}}_a$.

A second physical root of Eq. (6) appears for certain H once a local maximum of the cubic function at $x_{\max}^2 = a/3b^2$ shifts from large positive values to $x_{\max} < 1$. This takes place at $2(K + 2E) = 12K$ or $K/E = 0.4$. Since $f'(x) < 0$ for $x > x_{\max}$, the second root at $x_2 > x_{\max}$ is always a saddle point of the total energy $\mathcal{E}(x, H)$ (4). Hence, if the second solution with $0 < x_2 < 1$ is present, the magnetization cannot rotate continuously all the way between $\theta = 0$ and $\pi/2$ upon increasing H as it would lead to passing through the saddle point. Instead, at certain H_m there is a direct jump into the fully aligned state with $\theta = \pi/2$ ($x = 1$). Interestingly, transformation to the first-order magnetization

process occurs for relatively small values of higher-order anisotropy constants: $K > 0.4E$ or $K_2/K_1 < -1/6$.

The discussed behavior is illustrated in Fig. 2(a), which shows the magnetization component along the field computed by a numerical minimization of the classical energy (2) as well as by directly solving the cubic equation (5). For the threshold value $K/E = 0.4$ between second- and first-order magnetization processes $M(H)$ exhibits a pronounced upward curvature with the asymptotic behavior $M(H) \simeq \sqrt{H_m - H}$ near the saturation. The magnitude of the magnetization jump ΔM grows continuously above the threshold. Theoretical results for $\Delta M/M_s$, where M_s is the total magnetization, are shown in Fig. 2(b). Figure 2(c) illustrates a variation the transition field H_m for different K/E values.

An experimental value of the magnetization jump ΔM can be used to fix the ratio K/E in our model. The low-temperature magnetization measurements yield $\Delta M/M_s \sim 0.3$ for URhGe [35]. This jump value corresponds to $K/E \approx 0.7$ and $H_m \approx 2.82E$, see Fig. 2(b,c). For the magnetocrystalline anisotropy expansion (1) one finds accordingly $K_2 \approx -0.26K_1$. Hence, the experimental data yield a significantly smaller ratio of two anisotropy constants in comparison to the LSDA results [29]. From the experimental value of the transition field $H_m = 11.7$ T and ordered moments $M_s = g^* \mu_B \approx 0.41 \mu_B$ we obtain in the physical units: $E = g^* \mu_B H_m / 2.82 \approx 0.098$ meV or 1.14 K.

The uniaxial-stress measurements in magnetic field $H \parallel b$ observe a fast suppression of the transition field H_m for moderate stress σ_b applied along the b crystal axis [37]. In addition, the magnetization slope dM/dH rapidly increases with σ_b , whereas the Curie temperature T_C stays almost constant. Since both quantities H_m and dH/dM are set by the magnitude of the in-plane anisotropy constant, the experimental results suggest that E is strongly reduced by the b -axis stress. Such a behavior is consistent with a gradual restoration of structural isotropy in the bc plane by removing distortion of Rh-Ge hexagons, see Fig. 1. By the same token, K goes to zero as well, since the $\sin^4 \theta$ harmonic is also incompatible with the hexagonal rotation symmetry. On the other hand, the Curie temperature is set by exchange interactions between U atoms, which experience much weaker variations for $\sigma_b \lesssim 0.5$ GPa.

B. Tilted magnetic field

The second-order Ising transition is smeared once an external field rotates toward the easy axis. Still, the first-order metamagnetic transition remains stable for a range of tilting angles. The magnetization jump is continuously reduced and vanishes at a certain angle α^* . A high sensitivity of the reorientation transition H_m in URhGe to the magnetic field direction has been reported by a number of authors [34, 35].

Figure 3(a) shows the longitudinal magnetization

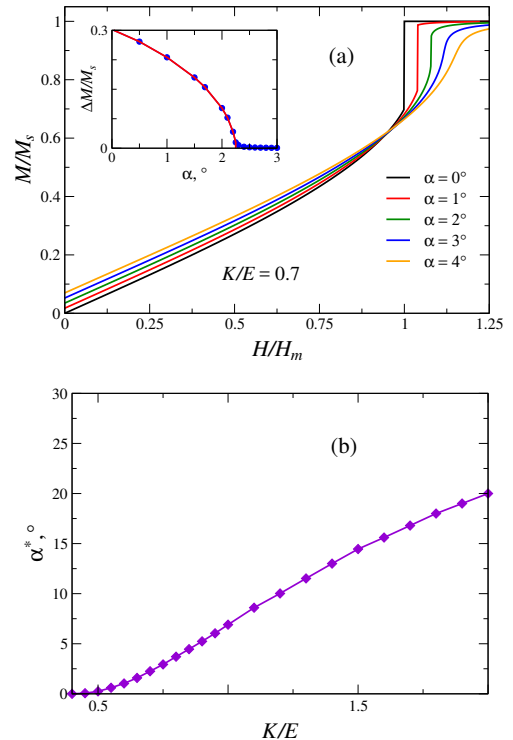


FIG. 3. (a) Magnetization curves for finite tilting angles α between an applied field and the b axis, $K = 0.7E$. The inset shows the tilting-angle dependence of the magnetization jump $\Delta M(\alpha)$ used to determine the critical angle α^* . (b) Dependence of the critical angle on the anisotropy constant.

$M_H = (\mathbf{M} \cdot \mathbf{H})/H$ in a tilted field $\tan \alpha = H_z/H_y$ obtained by numerical minimization of the energy (4) for $K/E = 0.7$. As the field tilting progresses, a magnitude of the magnetization jump is quickly suppressed. The jump vanishes at a critical point (α^*, H_m^*) on the first-order transition line $H_m(\alpha)$. By extrapolating $\Delta M(\alpha)$ to zero, we find the critical angle value $\alpha^* = 2.25^\circ$, see the inset in Fig. 3(a). The corresponding magnetic field is $H_m^* \approx 1.1H_m$ or 12.9 T in the dimensional units. Figure 3(b) shows the dependence of critical angle α^* on K/E .

The above theoretical values for α^* , H_m^* calculated with $K/E = 0.7$ are somewhat smaller than the experimental results $\alpha^* \approx 5^\circ$ and $H_m^* = 13.5$ T reported in Ref. [35]. The difference may be attributed to an unknown contribution of band electrons into M_s , which increases a relative value of the magnetization jump to be used in the spin model. Instead, K/E can be estimated from the experimental α^* , although measurements of the critical angle are not very precise. In addition, a higher order harmonic $K_3 \sin^6 \theta$ in the magnetic anisotropy (1) can play a role for URhGe, especially, under the uniaxial σ_b stress, which reduces the orthorhombic anisotropy, *i.e.*, K_1 and K_2 (E and K). Therefore, an inclusion of the corresponding term into \mathcal{H}_a may be necessary for a better fit of the experimental data. Since our aim in this work is to introduce a basic theoretical framework, we still consider the minimal spin model (2) with $K/E = 0.7$.

IV. FINITE TEMPERATURES

We now turn to the finite-temperature properties of the spin model (2), which have been studied using the classical Monte Carlo simulations. The standard Metropolis algorithm was combined with a restricted motion of spins in order to keep an acceptance rate at the level of 40–50%. Specifically, a trial spin orientation is randomly chosen on a spherical cap rather than on the whole sphere. The cap is centered on the initial spin direction and its height depends on temperature according to $\Delta S^z \simeq T$. In the present work we set the first 10^5 Monte Carlo steps at each temperature/field point for thermal equilibration and performed measurements over subsequent $5 \cdot 10^5$ steps. The Monte Carlo results were additionally averaged over 50–200 independent runs initialized by different random spin configurations. Such a procedure also provides an unbiased estimate of the statistical errors.

The analysis of Sec. IIIA allows us to fix the absolute values of the in-plane anisotropy constants E and K . In addition, the exchange parameter J can be inferred from the measured Curie temperature $T_C = 9.7$ K [17]. This step is complicated by the fact that magnetic anisotropy also affects the transition temperature. We have adopted the following procedure. URhGe has a dominant planar anisotropy, which places it in between the Heisenberg and the XY ferromagnets. For the latter two models, transition temperatures are, respectively, $T_c = 1.4429J$ [39] and $T_c = 2.2016J$ [40]. Bracketing T_c for the spin model (2) between these two values and using $E \approx 1.14$ K we obtain a relevant interval for $E/J \in (0.17, 0.3)$. A rough estimate $D/J = 3$ was also made based on the anisotropy of the magnetic susceptibility in the paramagnetic regime [37]. After that, a series of trial Monte Carlo runs was performed for various sets of microscopic constants in the chosen interval with the aim to fit the Curie temperature for URhGe. The obtained best parameter values are $E/J = 0.22$ and $J = 5.18$ K. A small value of E/J shows that URhGe is far from being an Ising ferromagnet as commonly assumed in the literature. Instead it has to be described as an XY ferromagnet with a weak in-plane anisotropy.

A. Zero magnetic field

The Monte Carlo simulations for the selected set of microscopic parameters have been performed on cubic clusters with $N = L^3$ spins and linear sizes $L = 8$ –40. Figure 4 shows the temperature dependence of the heat capacity C and the spontaneous magnetization $\langle |m_z| \rangle$ close to a phase transition. The λ -like anomaly in $C(T)$ gives a clear indication of the second-order phase transition at $T_c/J \sim 1.86$. A continuous rise of the ferromagnetic order parameter m_z below T_c further supports this conclusion. Still, the finite-size effects smear sharp singularities in the physical quantities and produce a rounding-off be-

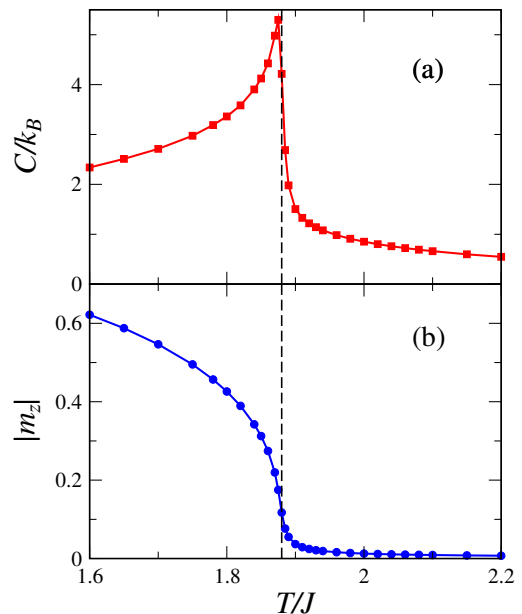


FIG. 4. Temperature dependence of (a) the specific heat and (b) the ferromagnetic magnetization for the spin model of URhGe with $E/J = 0.22$, $D/J = 3$, and $K/E = 0.7$ obtained for a spin cluster with $L = 36$. The vertical dashed line shows the position of the transition point at $T_c/J = 1.880$ in the thermodynamic limit $L \rightarrow \infty$.

havior near T_c for both $C(T)$ and $m_z(T)$. The specific heat peak is also slightly displaced away from the bulk T_c , see Fig. 4.

A precise location of the transition temperature T_c can be obtained using the fourth-order cumulant approach [41, 42]. The cumulants defined by

$$U_L = \frac{\langle m_z^4 \rangle}{\langle m_z^2 \rangle^2} \quad (7)$$

are computed for lattice clusters of different linear sizes L and plotted as a function of temperature, see Fig. 5(a). In the paramagnetic phase $T \gg T_c$ the fluctuations of the order parameter are gaussian and $U_L \approx 3$. Below T_c , the order parameter acquires a constant value and $U_L \approx 1$. Near the second-order transition, the finite-size scaling hypothesis [43] predicts that

$$U_L = \tilde{f}(L/\xi) = f(tL^{1/\nu}), \quad (8)$$

where $t = (T - T_c)/T_c$, $\xi \sim t^{-\nu}$ is a bulk correlation length, and $f(x)$ is a universal scaling function. According to the scaling law (8), the cumulant curves $U_L(T)$ cross at the critical temperature $t = 0$ of an infinite system $L \rightarrow \infty$ [41]. Additional small finite-size corrections to the leading scaling behavior can be taken into account by a proper extrapolation of the crossing points [39].

The transition temperature obtained from the crossing points of the fourth-order cumulants is $T_c/J = 1.880(1)$, which amounts to $T_C = 9.76$ K in excellent agreement

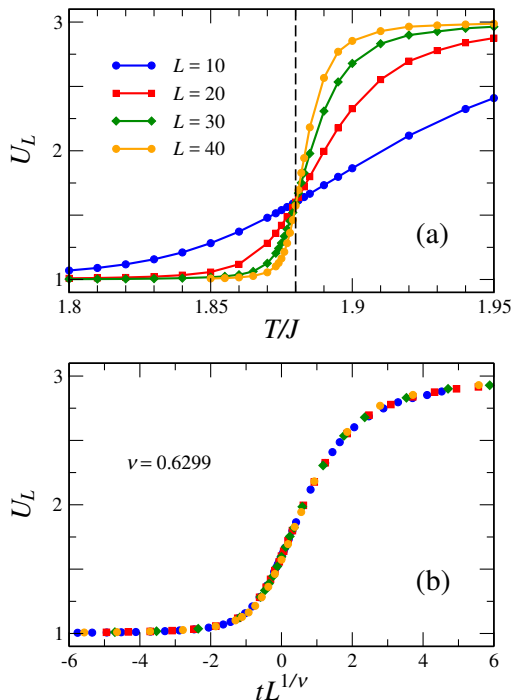


FIG. 5. The fourth-order cumulants $U_L(T)$ for different lattices as a function of (a) temperature and (b) the scaling variable $tL^{1/\nu}$. Same symbols are used to represent lattices with the same linear sizes L on both panels.

with the experimental value. We have also checked that despite a weakness of the in-plane anisotropy, $E \ll D$, the critical behavior of the spin model (2) still belongs to the 3D Ising universality class. For that we rescale the Monte Carlo data for $U_L(T)$ according to the scaling law (8) with the Ising critical exponent $\nu = 0.6299$ [44]. As a result, the data from different clusters collapse on the common curve given by $f(x)$, see Fig. 5(b). Additional scaling plots for the order parameter and the susceptibility that further verify the Ising values for $\beta = 0.3263$ and $\gamma = 1.2371$ are included in Appendix.

The critical properties of URhGe have been measured and discussed alongside with the experimental results for some other uranium ferromagnets in [45, 46]. The experimental values for the order-parameter exponent β are generally quite close to the 3D Ising value. On the other hand, the derived critical exponents γ and δ appear to be more mean-field like across the whole series of studied materials. The source of this discrepancy is currently not clear.

B. Tricritical point and phase diagram

Let us now consider the behavior in a magnetic field applied parallel to the b axis (y axis). Magnetization curves computed in the Monte Carlo simulations for a range of temperatures from $T/J = 0.1$ to 0.5 are shown in Fig. 6(a). The low-temperature curves demonstrate

clear jumps that signify a first-order transition between the polarized paramagnetic state at $H > H_m$ and the state with transverse ferromagnetic order at $H < H_m$. As temperature increases, height of the jump goes down and vanishes at a certain temperature. Nature of the phase transition changes from the first to the second order at such a tricritical point [47]. Tricritical points in the phase diagrams of the condensed matter systems have been the subject of theoretical and experimental investigations over several decades, see, for example, [48–66]. The mean-field Landau theory assigns the tricritical point to a point, where the quartic term coefficient pathes through zero [47, 51]. An Ising antiferromagnet in a longitudinal field provides an example of the tricritical point in the H – T diagram [55]. The tricritical point is also present in the p – T diagram of a metallic ferromagnet with a first-order quantum transition induced by soft fermionic modes [63–65].

In our Monte Carlo simulations, the tricritical point was located by extrapolating the magnetization jumps to zero $\Delta M \rightarrow 0$, as shown in Fig. 6(b). The extrapolation yields the tricritical temperature for the chosen set of parameters as $T_{tr} = 0.345(5)J$. With the previously deduced exchange constant $J = 5.18$ K, this corresponds to $T_{tr} = 1.79$ K. Our theoretical value is in a good agreement with $T_{tr} \approx 2$ K reported for URhGe in

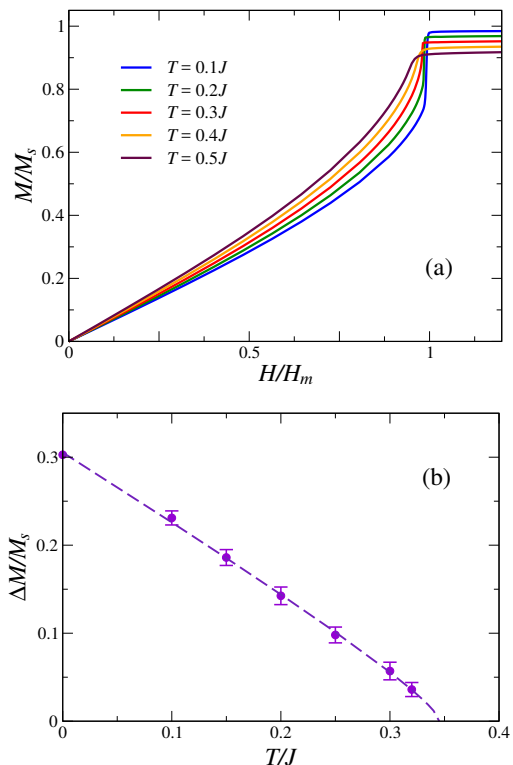


FIG. 6. (a) Low-temperature magnetization curves. Magnetic field is normalized to the value of the first-order transition field at $T = 0$: $H_m = 0.620J = 2.82E$. (b) Variation of the magnetization jump with temperature. The dashed line is an extrapolation curve used to determine T_{tr} .

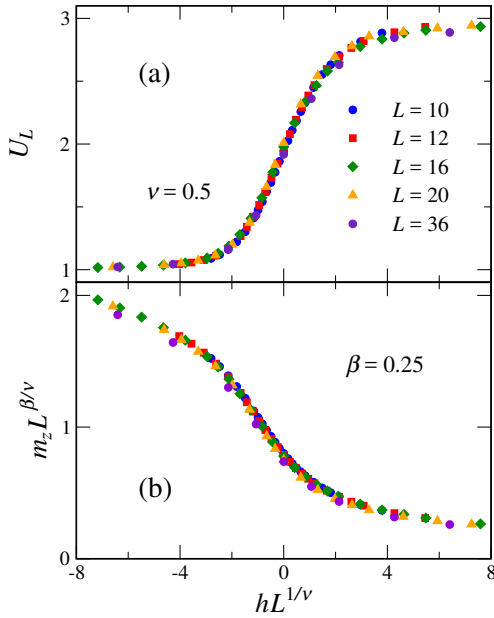


FIG. 7. Scaling plot for (a) the fourth-order cumulants $U_L(H)$ and (b) the order parameter m_z at $T = T_{\text{tr}}$. The tricritical mean-field exponents $\nu = 1/2$, $\beta = 1/4$ are used.

[20]. Magnetic field at the tricritical point was obtained from the crossing point of the fourth-order cumulants $U_L(H) = \langle m_z^4 \rangle / \langle m_z^2 \rangle^2$ ($H \parallel y$) computed at $T = T_{\text{tr}}$, similar to the procedure detailed in the preceding subsection for the zero-field transition. In units of the exchange constant the magnetic field value of the tricritical point is $H_{\text{tr}} = 0.607(1)J$. Taking into account that $H_m|_{T=0} = 2.82E = 0.62J$, this yields $H_{\text{tr}} = 11.4$ T.

Fluctuations near a tricritical point are generally stronger than those near a conventional second-order transition and are characterized by a nontrivial set of critical exponents already at the mean-field level [47, 51]:

$$\alpha = 1/2, \quad \beta = 1/4, \quad \gamma = 1, \quad \nu = 1/2. \quad (9)$$

The renormalization-group arguments indicate that these exponents remain valid for three-dimensional systems up to multiplicative logarithmic corrections [52–54]. Note that in our case the ‘specific heat’ exponent α applies to the second-order derivative of the thermodynamic potential $\partial^2 F / (\partial \zeta)^2 \simeq (\zeta - \zeta_{\text{tr}})^{-\alpha}$ along an arbitrary path $\zeta(T, H)$ in the T – H_y plane that crosses the transition line $H_m(T)$ under a finite angle. In particular, near the tricritical point the field derivative of the magnetization diverges with the mean-field exponent α [54]:

$$dM/dH = (H - H_{\text{tr}})^{-1/2}. \quad (10)$$

Such a square-root singularity is clearly seen in the behavior $M(H)$ shown in Fig. 6(a), though we do not attempt here a quantitative comparison.

We further verify the tricritical exponents β and ν by scaling the Monte Carlo results for $U_L(H)$ and $m_z(H)$

calculated for clusters with different linear sizes. The scaling parameter for an isothermal field scan is $hL^{1/\nu}$, where $h = (H - H_{\text{tr}})/H_{\text{tr}}$. The order parameter behavior in the critical region $m_z \simeq (H_{\text{tr}} - H)^\beta$, corresponds to a finite-size scaling form

$$m_z = L^{-\beta/\nu} g(hL^{1/\nu}). \quad (11)$$

Accordingly, the data for m_z need to be compensated by the cluster dependent factor $L^{\beta/\nu}$. The scaling plots for $U_L(H)$ and $m_z(H)$ are shown in Fig. 7. The data collapse quality is almost as good as for the zero-field transition despite the unaccounted logarithmic corrections. Overall, the Monte Carlo results of Fig. 7 provide a firm evidence that the tricritical point is characterized by the mean-field values $\beta = 1/4$ and $\nu = 1/2$. Note that the previous Monte Carlo studies have considered tricritical points for the Ising spin models only [58–62]. This work extends the numerical analysis of the tricritical behavior to a realistic spin Hamiltonian with three-component magnetic moments.

Our Monte Carlo data do not show any significant enhancement in the field-dependent heat capacity $C(H)$ as $H \rightarrow H_{\text{tr}}$ (or H_m). In contrast, a 20-25% rise of the specific heat between $H = 0$ and $H = H_m$ has been observed in experiment [34]. One possible explanation for this discrepancy is that the observed increase is entirely due to the conduction electrons either via a reconstruction of the Fermi surface [18–20] or via the effective mass enhancement.

After determining the location of the tricritical point, we ran the Monte Carlo simulations over a wide range of temperatures and magnetic fields. The constructed T – H diagram for $H \parallel y$ is shown in Fig. 8(a). The shape and position of a boundary surrounding the ferromagnetic phase closely resembles the experimental magnetic phase diagram of URhGe [20]. As soon as an applied field rotates in the easy plane away from the b axis, the c component of the field couples linearly to the order parameter and a wing-shaped phase diagram emerges from the tricritical point [50]. For URhGe such a phase diagram has been suggested in a number of experimental studies [33, 35]. In particular it has been argued that the quantum critical point, which terminates the line of first-order magnetic transitions in a tilted field, plays a key role for the field-induced superconducting phase [33].

Combining the Monte Carlo simulations with the energy minimization results of Sec. IIIB, we constructed the T – H_b – H_c phase diagram of URhGe, see Fig. 8(b). Essentially, we performed isothermal field scans for various values of the tilting angle α and extrapolated the magnetization jumps to zero in order to determine the critical angle $\alpha^*(T)$. Taking into account significant simulation times and multiple intermediate values of α to be explored, we were able to complete this procedure only for two temperatures between $T = T_{\text{tr}}$ and $T = 0$. The obtained phase diagram resembles qualitatively the expected behavior [33, 35, 50]. However, the limited number of points on the critical line $\alpha^*(T)$ does not allow

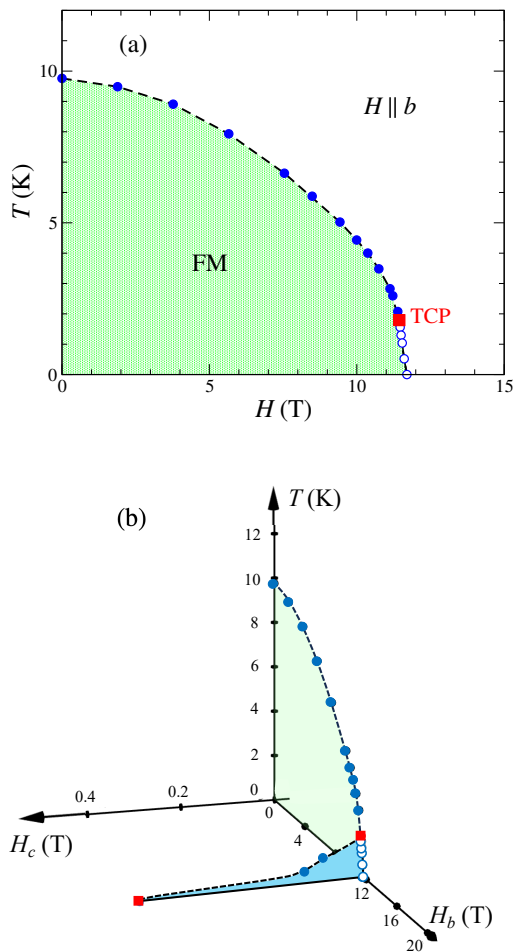


FIG. 8. (a) The Monte Carlo phase diagram of the anisotropic spin model for URhGe in a magnetic field parallel to the b axis. FM is a ferromagnetic phase. Closed circles and dashed lines indicate the continuous second-order transitions, open circles represent the first-order transitions. Red square marks the tricritical point (TCP). (b) The T - H_b - H_c phase diagram of URhGe. The blue surface corresponds to the plane of first-order transitions bounded at finite temperatures by a critical line $\alpha^*(T)$ that starts at TCP and extends down to $T = 0$ (second red square).

us to verify a tangential crossing of the transition lines, which is a general property of the wing-shaped diagrams discussed in [66].

V. DISCUSSION

We have formulated and investigated a minimal spin model that accounts for all basic properties of the heavy-fermion ferromagnet URhGe. The experimental values of the Curie temperature T_C , the reorientation field H_m , and the height of the magnetization jump have been used to fix the spin Hamiltonian parameters. For the chosen set of parameters we were able to *quantitatively* reproduce the other experimental features such as the critical

tilting angle α^* for $H \parallel bc$ plane, the position of the tricritical point (T_{tr}, H_{tr}), and the whole T - H_b phase diagram. This quantitative agreement supports our initial assumption that the magnetic subsystem in URhGe is described by a local moment model as opposed to the itinerant ferromagnetism scenarios.

The theoretical description of the magnetic phase diagram established in our work shows that URhGe has a moderately weak in-plane anisotropy $E/J \sim 0.22$. As a consequence, a gapped magnon mode representing transverse spin oscillations must be present in the ferromagnetic state. Further calculations of the dynamical magnetic susceptibility $\chi^{\alpha\beta}(\mathbf{q}, \omega)$ for URhGe can be performed on the basis of the Hamiltonian (2) using the precessional equation of motion for local magnetic moments. Information on $\chi^{\alpha\beta}(\mathbf{q}, \omega)$ is essential for the spin-fluctuation mechanism of the unconventional superconductivity, see [67] and references therein. Previously, a microscopic theory of the triplet superconducting phases in URhGe has been developed using a toy model for the magnetic subsystem [8]. Our study opens a way for more realistic theoretical calculations for the reentrant superconducting phase. Let us also mention that a promising route for deriving effective spin Hamiltonians similar to (2) has recently been discussed in the framework of the underscreened Kondo lattice model [68].

Overall, theoretical insights gained here can contribute to a broader understanding of magnetism in other uranium materials that exhibit metamagnetic transitions such as UIrGe [25], UCoAl [69], and UTe₂ [70]. In particular, UTe₂ has recently been the focus of numerous experimental and theoretical studies [71, 72]. In a spectacular parallel with the behavior of URhGe, UTe₂ remains superconducting up to a metamagnetic transition at $H_m = 35$ T ($H \parallel b$) with a large magnetization jump of $0.6\mu_B$ [70]. Magnetic properties of UTe₂ are dominated by relatively large local moments $\sim 3\mu_B$ on U atoms [72]. However, the material remains paramagnetic down to the lowest studied temperatures. The inelastic neutron-scattering measurements unveil a complex pattern of coexisting antiferro- and ferromagnetic fluctuations in UTe₂ [73]. Therefore, in addition to anisotropy, a realistic spin model for this material should include competing frustrated exchange interactions. The development of the microscopic description for UTe₂, as well as for other metamagnetic uranium materials, is undoubtedly an interesting open problem.

ACKNOWLEDGMENTS

We are grateful to D. Aoki, D. Braithwaite, J.-P. Brison, A. Huxley, G. Knebel, F. Lévy, V. P. Mineev, and T. Ziman for useful and inspiring discussions and other help. The financial support was provided by the French Research Agency (ANR), within the project FRESCO, Project No. ANR-20-CE30-0020.

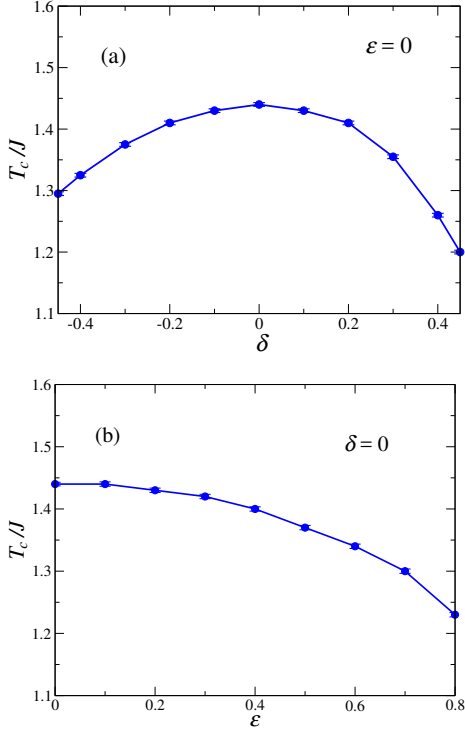


FIG. 9. Dependence of the transition temperature of the classical Heisenberg spin model on an orthorhombic distortion (a) δ and (b) ϵ , see (A2) for notations.

Appendix A

In Appendix we include the Monte Carlo data in support of the conclusions reached in the main text.

First, we consider an effect of orthorhombic pattern of exchange couplings on the transition temperature of a classical Heisenberg ferromagnet. For a simple cubic lattice model with the nearest-neighbor exchange J , the transition temperature is $T_c = 1.4429J$ [39]. In an orthorhombic case, the exchange interactions may differ along the three orthogonal directions:

$$\hat{\mathcal{H}} = -\frac{1}{2} \sum_{i,\rho} J_\rho \mathbf{S}_i \cdot \mathbf{S}_{i\pm\rho}, \quad (\text{A1})$$

where $\rho = x, y, z$. It is convenient to normalize the exchange constants to an average value $J = (J_x + J_y + J_z)/3$. The remaining ‘orthorhombic distortion’ can be generally parametrized as

$$J_z/J = 1 + 2\delta, \quad J_{x,y}/J = 1 - \delta \pm \epsilon. \quad (\text{A2})$$

Using the Monte Carlo simulations we have determined the transition temperature for two slices of the surface $T_c(\delta, \epsilon)$: $\epsilon = 0$ and $\delta = 0$.

Figure 9(a) shows variations of the transition temperature between a layered ferromagnet with $J_z : J_{x,y} = 0.1 : 1.45$ ($\delta = -0.45$) and a model with weakly coupled chains $J_z : J_{x,y} = 1.9 : 0.55$ ($\delta = 0.45$). In the

second case, all three exchanges are different with the ratios $J_z : J_x : J_y = 1 : 1.8 : 0.2$ for $\epsilon = 0.8$, see Fig. 9(b). Overall, the highest transition temperature is always achieved for an ideal cubic structure. Also, the quasi one-dimensional distortion of the exchange parameters results in a stronger suppression of T_c in comparison to the quasi two-dimensional pattern of exchanges. However, the transition temperature variations do not exceed 10–20% even for the limiting cases. Hence, the transition temperature of an orthorhombic ferromagnet, like URhGe, is mainly determined by an average exchange J and has a little dependence on a specific spatial distribution of J_ρ .

Second, we consider the spin model of URhGe (2) for the chosen set of the microscopic parameters and present the zero-field scaling plots for the order parameter $m_z \propto t^\beta$ and the magnetic susceptibility $\chi^{zz} = dm_z/dH_z \propto t^{-\gamma}$ with $t = (T - T_c)/T_c$. The scaling theory predicts the following singularities for finite systems:

$$m_z = L^{-\beta/\nu} g_1(tL^{1/\nu}), \quad \chi^{zz} = L^{\gamma/\nu} g_2(tL^{1/\nu}), \quad (\text{A3})$$

where $g_1(x)$ and $g_2(x)$ are the universal functions. The Monte Carlo simulation results are presented in Fig. 10 and show a nice collapse of the data from different clusters on the common curves for the 3D Ising set of the critical exponents.

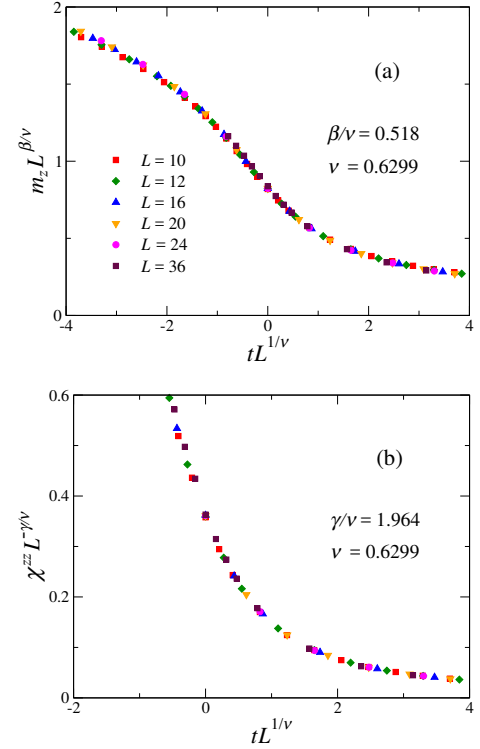


FIG. 10. Zero field scaling plots for the easy-axis magnetization m_z (a) and the uniform susceptibility χ^{zz} (b) for different lattice sizes L with the 3D Ising critical exponents, $t = (T - T_c)/T_c$ and $T_c/J = 1.88$. Same symbols are used to represent lattices with the same linear sizes L on both panels.

-
- [1] S. S. Saxena, P. Agarwal, K. Ahilan, F. M. Grosche, R. K. W. Hasselwimmer, M. J. Steiner, E. Pugh, I. R. Walker, S. R. Julian, P. Monthoux, G. G. Lonzarich, A. Huxley, I. Sheikin, D. Braithwaite, J. Flouquet, Superconductivity on the border of itinerant-electron ferromagnetism in UGe_2 , *Nature* **406**, 587 (2000).
- [2] D. Aoki, A. Huxley, E. Ressouche, D. Braithwaite, J. Flouquet, J.-P. Brison, E. Lhotel, and C. Paulsen, Coexistence of superconductivity and ferromagnetism in URhGe , *Nature* **413**, 613 (2001).
- [3] N. T. Huy, A. Gasparini, D. E. de Nijs, Y. Huang, J. C. P. Klaasse, T. Gortenmulder, A. de Visser, A. Hamann, T. Görlach, and H. v. Löhneysen, Superconductivity on the border of weak itinerant ferromagnetism in UCoGe , *Phys. Rev. Lett.* **99**, 067006 (2007).
- [4] K. G. Sandeman, G. G. Lonzarich, and A. J. Schofield, Ferromagnetic superconductivity driven by changing Fermi surface topology, *Phys. Rev. Lett.* **90**, 167005 (2003).
- [5] N. Karchev, Magnon exchange mechanism of ferromagnetic superconductivity, *Phys. Rev. B* **67**, 054416 (2003).
- [6] A. H. Nevidomskyy, Coexistence of ferromagnetism and superconductivity close to a quantum phase transition: the Heisenberg- to Ising-type crossover, *Phys. Rev. Lett.* **94**, 097003 (2005).
- [7] V. P. Mineev, Magnetic field dependence of pairing interaction in ferromagnetic superconductors with triplet pairing, *Phys. Rev. B* **83**, 064515 (2011).
- [8] K. Hattori and H. Tsunetsugu, *P*-wave superconductivity near a transverse saturation field, *Phys. Rev. B* **87**, 064501 (2013).
- [9] L. Bulaevskii, R. Eneias, and A. Ferraz, Triplet superconductivity in ferromagnets due to magnon exchange, *Phys. Rev. B* **99**, 064506 (2019).
- [10] V. P. Mineev, Upper critical field in ferromagnetic metals with triplet pairing, *Ann. Phys. (NY)* **417**, 168139 (2020).
- [11] A. D. Huxley, Ferromagnetic superconductors, *Physica C* **514**, 368 (2015).
- [12] V. P. Mineev, Superconductivity in uranium ferromagnets, *Phys. Usp.* **60**, 121 (2017).
- [13] D. Aoki, K. Ishida, and J. Flouquet, Review of U-based ferromagnetic superconductors: comparison between UGe_2 , URhGe , and UCoGe , *J. Phys. Soc. Jpn.* **88**, 022001 (2019).
- [14] F. Lévy, I. Sheikin, B. Grenier, and A. D. Huxley, Magnetic field-induced superconductivity in the ferromagnet URhGe , *Science* **309**, 1343 (2005).
- [15] V. Sechovsky and L. Havela, Magnetism of Ternary Intermetallic Compounds of Uranium, *Handbook of Magnetic Materials*, vol. 11, p. 1, ed. K. H. J. Buschow (Elsevier, Amsterdam, 1998).
- [16] P. Fulde, P. Thalmeier, and G. Zwicknagl, Strongly Correlated Electrons, in *Solid State Physics*, vol. 60, p. 1, eds. H. Ehrenreich and D. Turnbull (Academic Press, San Diego, 2006).
- [17] S. Sakarya, N. H. van Dijk, A. de Visser, and E. Brück, Dilatometry study of the ferromagnetic order in single-crystalline URhGe , *Phys. Rev. B* **67**, 144407 (2003).
- [18] E. A. Yelland, J. M. Barraclough, W. Wang, K. V. Kamenev, and A. D. Huxley, High-field superconductivity at an electronic topological transition in URhGe , *Nature Phys.* **7**, 890 (2011).
- [19] D. Aoki, G. Knebel, and J. Flouquet, Fermi surface instabilities in ferromagnetic superconductor URhGe , *J. Phys. Soc. Jpn.* **83**, 094719 (2014).
- [20] A. Gourgout, A. Pourret, G. Knebel, D. Aoki, G. Seyfarth, and J. Flouquet, Collapse of ferromagnetism and Fermi surface instability near reentrant superconductivity of URhGe , *Phys. Rev. Lett.* **117**, 046401 (2016).
- [21] Y. Sherkunov, A. V. Chubukov, and J. J. Betouras, Effects of Lifshitz transitions in ferromagnetic superconductors: the case of URhGe , *Phys. Rev. Lett.* **121**, 097001 (2018).
- [22] W. Müller, V. H. Tran, and M. Richter, Cancellation of spin and orbital moments in URhGe under pressure: a density-functional prediction, *Phys. Rev. B* **80**, 195108 (2009).
- [23] F. Wilhelm, J.-P. Sanchez, J.-P. Brison, D. Aoki, A. B. Shick, and A. Rogalev, Orbital and spin moments in the ferromagnetic superconductor URhGe by x-ray magnetic circular dichroism, *Phys. Rev. B* **95**, 235147 (2017).
- [24] K. Prokes, T. Tahara, Y. Echizen, T. Takabatake, T. Fujita, I. H. Hagmusa, J. C. P. Klaasse, E. Brück, F. R. de Boer, M. Divis, V. Sechovsky, Electronic properties of a URhGe single crystal, *Physica B* **311**, 220 (2002).
- [25] S. Yoshii, A. V. Andreev, E. Brück, J. C. P. Klaasse, K. Prokes, F. R. de Boer, M. Hagiwara, K. Kindo, and V. Sechovsky, Magnetization and specific heat of a URhGe single crystal in high magnetic fields, *J. Phys. Conf. Series* **51**, 151 (2006).
- [26] S. Sachdev, *Quantum phase transitions*, (Cambridge Univ. Press, Cambridge, 2011).
- [27] G. Asti, First-order magnetic processes, in *Ferromagnetic Materials*, vol. 5, p. 397, eds. K.H.J. Buschow and E.P. Wohlfarth (North-Holland, Amsterdam, 1990).
- [28] D. Melville, W. I. Khan, and S. Rinaldi, First order magnetisation processes in $\text{Pr}_2(\text{Co}_{1-x}\text{Fe}_x)_{17}$ alloys, *IEEE Trans. Magn.* **12**, 1012 (1976).
- [29] A. B. Shick, Electronic and magnetic structure of URhGe , *Phys. Rev. B* **65**, 180509 (2002).
- [30] V. P. Mineev, Interplay between magnetism and superconductivity in URhGe , *C. R. Physique* **7**, 35 (2006).
- [31] V. P. Mineev, Metamagnetic phase transition in the ferromagnetic superconductor URhGe , *Phys. Rev. B* **103**, 144508 (2021).
- [32] A. Huxley, unpublished.
- [33] F. Lévy, I. Sheikin, and A. Huxley, Acute enhancement of the upper critical field for superconductivity approaching a quantum critical point in URhGe , *Nature Phys.* **3**, 460 (2007).
- [34] F. Lévy, I. Sheikin, B. Grenier, C. Marcenat, and A. Huxley, Coexistence and interplay of superconductivity and ferromagnetism in URhGe , *J. Phys.: Cond. Matter* **21**, 164211 (2009).
- [35] S. Nakamura, T. Sakakibara, Y. Shimizu, S. Kittaka, Y. Kono, Y. Haga, J. Pospíšil, and E. Yamamoto, Wing structure in the phase diagram of the Ising ferromagnet URhGe close to its tricritical point investigated by angle-resolved magnetization measurements, *Phys. Rev. B* **96**, 094411 (2017).
- [36] K. H. J. Buschow and F. R. de Boer, *Physics of Mag-*

- netism and Magnetic Materials* (Kluwer Academic, New York, 2003).
- [37] D. Braithwaite, D. Aoki, J.-P. Brison, J. Flouquet, G. Knebel, A. Nakamura, and A. Pourret, Dimensionality driven enhancement of ferromagnetic superconductivity in URhGe, *Phys. Rev. Lett.* **120**, 037001 (2018).
 - [38] K. Prokes, T. Tahara, Y. Echizen, T. Takabatake, T. Fujita, I. H. Hagmusa, J. C. P. Klaass E. Brück, F. R. de Boer, M. Divis, V. Sechovsky, Erratum to “Electronic properties of an URhGe single crystal”, *Physica B* **334**, 272 (2003).
 - [39] K. Chen, A. M. Ferrenberg, and D. P. Landau, Static critical behavior of three-dimensional classical Heisenberg models: a high-resolution Monte Carlo study, *Phys. Rev. B* **48**, 3249 (1993).
 - [40] M. Hasenbusch and S. Meyer, Critical exponents of the 3D XY model from cluster update Monte Carlo, *Phys. Lett. B* **241**, 238 (1990).
 - [41] K. Binder, Finite-size scaling analysis of Ising model block distribution functions, *Z. Phys. B* **43**, 119 (1981).
 - [42] K. Binder and D. W. Heermann, *Monte Carlo Simulations in Statistical Physics* (Springer-Verlag, Berlin, 1988).
 - [43] M. N. Barber, Finite-size scaling, *Phase Transitions and Critical Phenomena*, vol. 8, p. 146, edited by C. Domb and J. L. Lebowitz (Academic, New York, 1983).
 - [44] A. M. Ferrenberg, J. Xu, and D. P. Landau, Pushing the limits of Monte Carlo simulations for the three-dimensional Ising model, *Phys. Rev. E* **97**, 043301 (2018).
 - [45] N. Tateiwa, Y. Haga, T. D. Matsuda, E. Yamamoto, and Z. Fisk, Unconventional critical scaling of magnetization in ferromagnetic uranium superconductors UGe₂ and URhGe, *Phys. Rev. B* **89**, 064420 (2014).
 - [46] N. Tateiwa, Y. Haga, and E. Yamamoto, Novel critical behavior of magnetization in URhSi: similarities to the uranium ferromagnetic superconductors UGe₂ and URhGe, *Phys. Rev. B* **99**, 094417 (2019).
 - [47] L. D. Landau and E. M. Lifshitz, *Statistical Physics I* (Pergamon Press, Oxford, 1980).
 - [48] R. B. Griffiths, Thermodynamics near the two-fluid critical mixing point in He³-He⁴, *Phys. Rev. Lett.* **24**, 715 (1970).
 - [49] C. Vettier, H. L. Alberts, and D. Bloch, Tricritical lines in metamagnets, *Phys. Rev. Lett.* **31**, 1414 (1973).
 - [50] R. B. Griffiths, Proposal for notation at tricritical points, *Phys. Rev. B* **7**, 545 (1973).
 - [51] J. M. Kincaid and E. G. D. Cohen, Phase diagrams of liquid helium mixtures and metamagnets: experiment and mean field theory, *Phys. Rep.* **22**, 57 (1975).
 - [52] F. J. Wegner and E. K. Riedel, Logarithmic corrections to the molecular-field behavior of critical and tricritical systems, *Phys. Rev. B* **7**, 248 (1973).
 - [53] M. J. Stephen, E. Abrahams, J. P. Straley, Logarithmic corrections to the mean-field theory of tricritical points, *Phys. Rev. B* **12**, 256 (1975).
 - [54] M. E. Fisher and S. Sarbach, Nonuniversality of tricritical behavior, *Phys. Rev. Lett.* **41**, 1127 (1978).
 - [55] E. Strykowski and N. Giordano, Metamagnetism, *Adv. Phys.* **26**, 487 (1977).
 - [56] E. I. Gerzanich and V. M. Fridkin, Tricritical points in ferroelectrics, *Ferroelectrics* **31**, 127 (1981).
 - [57] T. A. L. Ziman, D. J. Amit, G. Grinstein, and C. Jayaprakash, Renormalization-group study of the critical end point in $4 - \epsilon$ dimensions, *Phys. Rev. B* **25**, 319 (1982).
 - [58] D. P. Landau, Tricritical exponents and crossover behavior of a next-nearest-neighbor Ising antiferromagnet, *Phys. Rev. B* **14**, 4054 (1976).
 - [59] H. T. Diep, S. Galam, and P. Azaria, Three-dimensional dilute Ising antiferromagnet in a field: tricritical point and next-nearest neighbours, *EPL* **4**, 1067 (1987).
 - [60] H. J. Herrmann and D. P. Landau, Stability of the tricritical point in a three-dimensional next-nearest-neighbor Ising antiferromagnet: a Monte Carlo simulation, *Phys. Rev. B* **48**, 239 (1993).
 - [61] R. Ren, C. J. O’Keeffe, and G. Orkoulas, Simulation of symmetric tricritical behavior in electrolytes, *J. Chem. Phys.* **125**, 124504 (2006).
 - [62] J. B. dos Santos-Filho, D. F. de Albuquerque, and N. O. Moreno, Magnetic properties of the metamagnet Ising model in a three-dimensional lattice in a random and uniform field, *J. Phys.: Conf. Ser.* **249**, 012039 (2010).
 - [63] D. Belitz, T. R. Kirkpatrick, and T. Vojta, First order transitions and multicritical points in weak itinerant ferromagnets, *Phys. Rev. Lett.* **82**, 4707 (1999).
 - [64] T. R. Kirkpatrick and D. Belitz, Universal low-temperature tricritical point in metallic ferromagnets and ferri-magnets, *Phys. Rev. B* **85**, 134451 (2012).
 - [65] M. Brando, D. Belitz, F. M. Grosche, and T. R. Kirkpatrick, Metallic quantum ferromagnets, *Rev. Mod. Phys.* **88**, 025006 (2016).
 - [66] V. Taufour, U. S. Kaluarachchi, and V. G. Kogan, Constraints on the merging of the transition lines at the tricritical point in a wing-structure phase diagram, *Phys. Rev. B* **94**, 060410(R) (2016).
 - [67] P. Monthoux, D. Pines, and G. G. Lonzarich, Superconductivity without phonons, *Nature* **450**, 1177 (2007).
 - [68] E. Scott and M. Kwasigroch, Universal properties of residual moments in heavy-fermion metals, preprint [arXiv:2407.01218](https://arxiv.org/abs/2407.01218).
 - [69] T. D. Matsuda, N. Tateiwa, E. Yamamoto, Y. Haga, Y. Onuki, D. Aoki, J. Flouquet, and Z. Fisk, Magnetic phase diagram of UCoAl, *J. Kor. Phys. Soc.* **63**, 575 (2013).
 - [70] A. Miyake, Y. Shimizu, Y. J. Sato, D. Li, A. Nakamura, Y. Homma, F. Honda, J. Flouquet, M. Tokunaga, and D. Aoki, Metamagnetic transition in heavy fermion superconductor UTe₂, *J. Phys. Soc. Jpn.* **88**, 063706 (2019).
 - [71] D. Aoki, J.-P. Brison, J. Flouquet, K. Ishida, G. Knebel, Y. Tokunaga, and Y. Yanase, Unconventional superconductivity in UTe₂, *J. Phys.: Condens. Matter* **34**, 243002 (2022).
 - [72] S. K. Lewin, C. E. Frank, S. Ran, J. Paglione, and N. P. Butch, A review of UTe₂ at high magnetic fields, *Rep. Prog. Phys.* **86**, 114501 (2023).
 - [73] W. Knafo, G. Knebel, P. Steffens, K. Kaneko, A. Rosuel, J.-P. Brison, J. Flouquet, D. Aoki, G. Lapertot, and S. Raymond, Low-dimensional antiferromagnetic fluctuations in the heavy-fermion paramagnetic ladder compound UTe₂, *Phys. Rev. B* **104**, L100409 (2021).